Journal of Engineering Issues and Solutions

Effect of Rayleigh Damping Variation on the Seismic Fragility of Masonry Structures

Magnus Upadhyay[1], Pradeep Kafle[1], Sabin Ban[2], and Shreedhar Khakurel[1*]

[1] *Pashchimanchal Campus, Institute of Engineering, Tribhuvan University, Nepal.*
[2] *National College of Engineering, Institute of Engineering, Tribhuvan University, Nepal.*
**Corresponding email: shreedhar.khakurel@ioepas.edu.np*
Received: November 25, 2025; Revised: 27 January, 2026; Accepted: March 21, 2026

Abstract

Masonry structures in earthquake-prone areas are highly vulnerable because they are often built with weak materials, poor detailing, and limited maintenance, yet their seismic behavior is still not well studied. Damping is one of the parameters that influences seismic performance. It plays a critical role in energy dissipation, but its effect on masonry fragility is not fully understood. This study focuses on the influence of Rayleigh damping variation on the seismic fragility of unreinforced masonry (URM) and reinforced masonry (RM) buildings using a numerical macro-modeling approach. Nonlinear dynamic responses were analyzed under damping ratios ranging from 1% to 6%, and incremental dynamic analyses (IDA) were performed to generate corresponding fragility curves for each damping level. Results show that with an increase in damping ratios there was a reduction in roof displacements and overall seismic response, with URM showing strong sensitivity to Rayleigh damping variation. In contrast to this, RM structures exhibited reduced sensitivity, with damping effects decreasing toward collapse states. Across all damage states, reinforced masonry consistently outperformed unreinforced masonry. These findings showed the need for site- and material-specific damping characterization for URM, whereas standard guideline-based damping ratios are generally sufficient for RM, even at collapse-level fragility. The study highlights the importance of evaluating damping sensitivity in seismic fragility assessments and contributes to improving the reliability of numerical modeling for masonry structures.

Keywords: *Fragility, Incremental Dynamic Analysis, Masonry Structure, Rayleigh Damping*

1. Introduction

Earthquakes show a consistent threat to human life and infrastructure across the globe, particularly in seismically active regions such as Japan, Chile, Italy, Turkey, Greece, and Nepal (D'Alessandro & Fusi, 2025). These countries frequently experience moderate to large earthquakes, emphasizing the global importance of understanding and improving structural resilience (Acharya et al., 2024). Due to its seismically active geology, Nepal has also experienced numerous catastrophic earthquakes with magnitudes exceeding Mw 7.5 throughout its history, including those in 1255, 1408, 1505, 1833, 1934, and 2015 (Ram & Wang, 2013). In

recent years, the 2015 Gorkha earthquake (Mw 7.8) and the 2023 Jajarkot earthquake (Mw 5.7) have further highlighted the country's vulnerability.

Masonry structures in such earthquake-prone regions are especially vulnerable due to inadequate materials, weak structural detailing, and poor maintenance, conditions often linked to limited resources and lack of seismic design awareness (Ortega et al., 2019). Masonry structures, particularly unreinforced masonry (URM), dominate the rural building stock and have been severely affected during these events (Adhikari & D'Ayala, 2020). URM has been the primary construction material in the Nepal Himalayas since ancient times, often built with or without mud mortar depending on local practices (Khadka, 2020). A post-earthquake damage assessment conducted after the 2015 Gorkha event across fourteen severely affected districts revealed that two-story stone masonry buildings were the most common type. This is due to locally available and inexpensive materials; however, these structures suffered extensive damage and were responsible for many casualties (Wang et al., 2018). Masonry construction remains widespread worldwide and particularly in Nepal. It continues to be underrepresented in seismic research because of its complex behavior and modeling challenges (Jaishi et al., 2003). Among the various parameters affecting its seismic performance, damping is one of the most critical. Nevertheless, it is also one of the least explored, as it governs the energy dissipation characteristics of masonry under dynamic loading (Jaishi et al., 2003).

The accurate characterization of the dynamic properties of masonry structures is important for studying their seismic load-carrying capacity in future earthquakes. However, available data on their actual dynamic behavior remain limited and often lack focused investigation (Jaishi et al., 2003). In numerical seismic simulations, equivalent viscous damping is commonly introduced to represent the complex mechanisms of energy dissipation that occur through cracking, friction, and material degradation during seismic excitation. Among various formulations, Rayleigh damping remains the most widely adopted approach because of its simplicity and compatibility with conventional finite-element and macro-modeling platforms (Alipour & Zareian, 2008).

Rayleigh damping is defined by the matrix as a linear combination of the mass and stiffness matrices, with two coefficients, a_0 and a_1, representing the contribution of low- and high-frequency modes, respectively (Chopra, 2012). Although this formulation is convenient, selecting appropriate Rayleigh coefficients is challenging (Alipour & Zareian, 2008). Improper selection of these parameters can result in unrealistic energy dissipation, distorted modal properties, and biased structural response amplitudes (Hall, 2006). Since masonry structures inherently exhibit nonlinear and damage-dependent behavior, the sensitivity of their seismic response to damping variation is likely to be even more pronounced (Jaishi et al., 2003). Nonlinearities—whether geometric or material—must therefore be properly addressed in seismic analysis. Direct time integration with Rayleigh damping provides one of the most effective means to capture these effects and to realistically simulate the dynamic response of structures under earthquake loading (Spears & Jensen, 2012).

The behavior and application of Rayleigh damping in seismic analysis have been discussed for different structural systems. Several studies have examined its use in tall buildings and general structural models, addressing coefficient estimation, modeling limitations, and issues related to energy dissipation (Cruz & Miranda, 2017a, 2017b; Hall, 2006; Rahman & Gupta, 2020). For masonry systems, Galvez et al. (2022) investigated damping considerations in rocking block dynamics, providing partial insight into the damping characteristics of unreinforced masonry (URM).

In parallel, progress has been made in the development of fragility functions for masonry structures in Nepal, through both analytical and observational approaches (Gautam, 2018; Giordano et al., 2021; Guragain et al.,

2012). These studies have contributed significantly to understanding masonry vulnerability under seismic loading. However, despite these contributions, the sensitivity of masonry fragility to variations in Rayleigh damping parameters remains insufficiently understood. While Rayleigh damping is widely used in nonlinear dynamic analyses, its potential influence on fragility outcomes remains an open area of investigation. A focused study on this aspect can improve the reliability of fragility-based seismic assessments and deepen the understanding of damping sensitivity in masonry structures.

The primary objective of this study is to examine the influence of Rayleigh damping variation on the seismic fragility of unreinforced masonry (URM) and reinforced masonry (RM) buildings. For this, a numerical macro-modeling approach is followed. The nonlinear dynamic response of masonry structures is analyzed under varying damping ratios, ranging from 1% to 6%. For each damping level, incremental dynamic analysis (IDA) is performed to generate corresponding fragility curves, enabling a comparative assessment of how variations in Rayleigh damping parameters influence the damage probability of masonry buildings.

2. Building Description

Following the 2015 Gorkha earthquake in Nepal, the Department of Urban Development and Building Construction (DUDBC) published a catalogue featuring eight stone masonry building models for reconstruction purposes. In this study, the geometric configuration of the SMC 2.3 model from the DUDBC (DUDBC, 2015a) catalogue was used as a reference. Based on its geometry, two analytical models—an unreinforced masonry (URM) model and a reinforced model (RM)—were developed for further numerical investigation. The plan and front elevation of the building is presented in Figure 1.

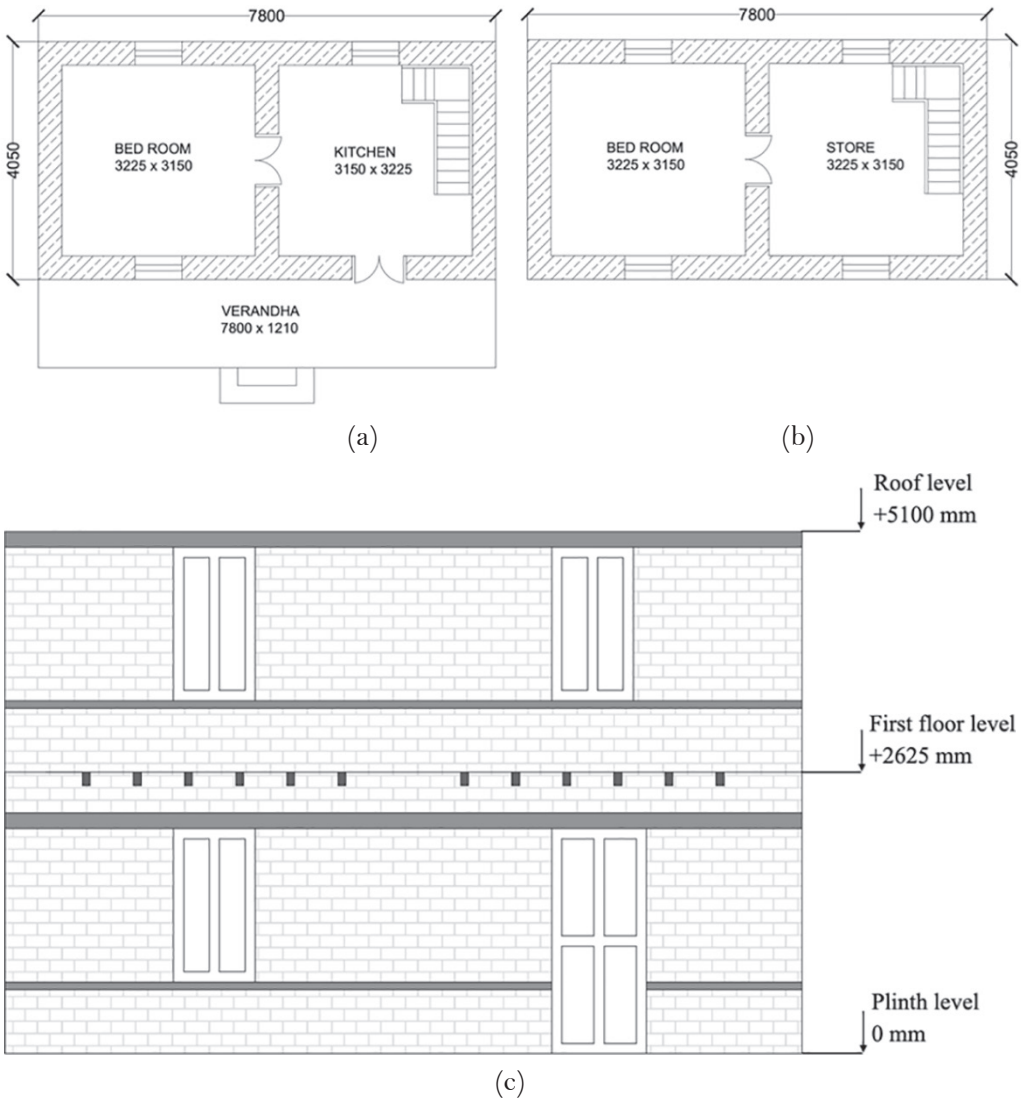

Figure 1: (a) Ground floor plan, **(b)** First floor plan, and **(c)** Front elevation of representative building

The URM model represents stone units bonded with mud mortar, which forms a typical stone–mud masonry structure. It includes timber beams and timber flooring with loose connections, which act as flexible diaphragms. This model does not incorporate any specific seismic-resisting elements.

The RM model comprises the same stone–mud masonry with additional seismic strengthening elements. Sill, lintel, and roof bands were modeled using M20-grade concrete (28-day characteristic cube compressive strength of 20 MPa), reinforced with Fe415 steel (yield strength = 415 MPa). Each band was provided with 12 mm longitudinal bars and 6 mm diameter stirrups placed at 150 mm center-to-center spacing. Furthermore, a 16 mm diameter vertical reinforcement bar was provided at each wall junction. All reinforcement details and configurations follow the provisions of NBC 202: 2015 (NBC, 2015; DUDBC, 2015a).

Figure 2 illustrate the cross-sectional arrangements of the sill, and lintel bands (all dimensions in mm). The lightweight roof structure was not explicitly modeled; however, its self-weight was computed and applied as a uniformly distributed load along the top of the walls.

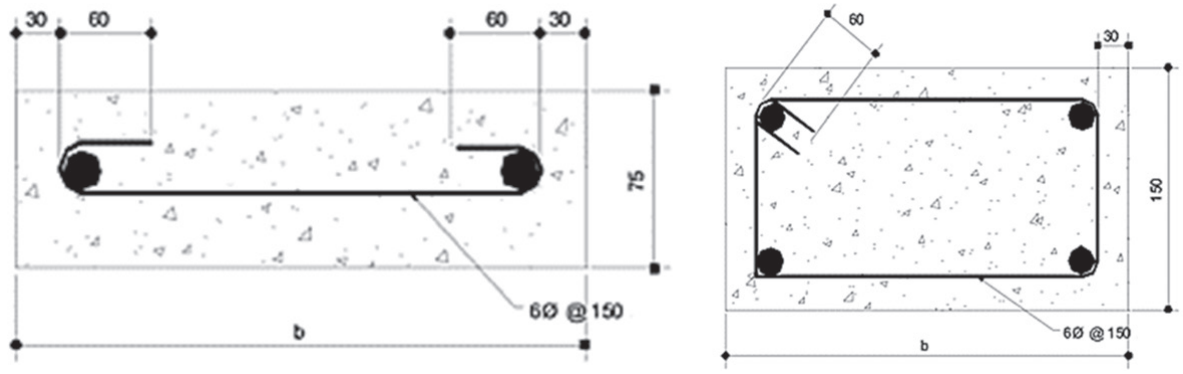

(a) (b)

Figure 2: (a) Sill Band, (b) Lintel Band (NBC, 2015)

3. Numerical Modeling

Three-dimensional finite element–based numerical models (macro-models) were developed using the *DIANA FEA 10.5* software (DIANA, 2020). Two models were analyzed: (1) Unreinforced Stone Mud Masonry (URM), as shown in Figure 3(a), and (2) Reinforced Stone Mud Masonry (RM), as shown in Figure 3(b). Each model was analyzed for varying damping ratios ranging from 1% to 6%.

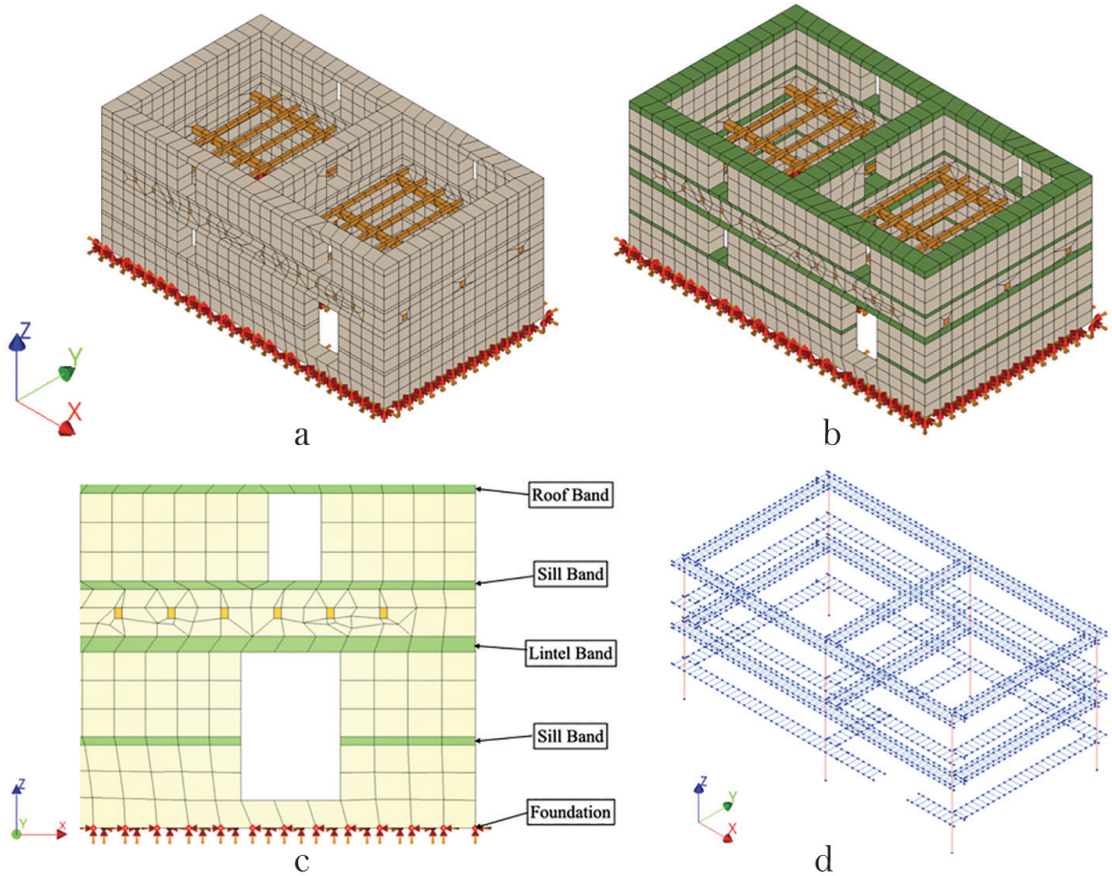

Figure 3: (a) URM FE model **(b)** RM FE model **(c)** Band detail in RM model **(d)** Reinforcement adopted in RM model

Solid elements were classified as structural solids, with the Total Strain-Based Crack Model adopted to represent the nonlinear material behavior of masonry walls. Also, a rotating crack orientation approach was employed while the tensile response followed an exponential softening law, with the crack bandwidth defined as per Rots. Finally, the compressive response was modeled using a parabolic stress–strain relationship as shown in Figure 4.

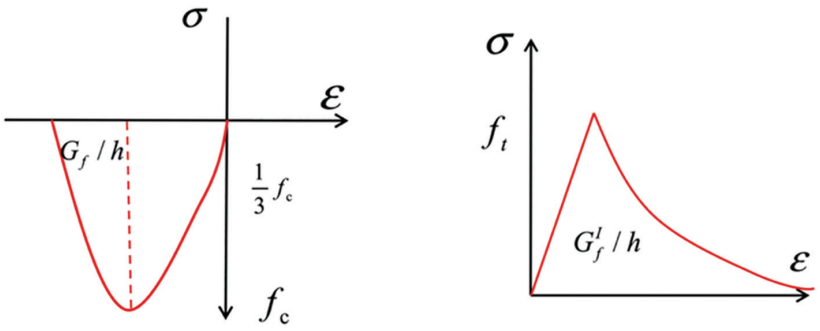

(a) (b)

Figure 4: Masonry constitutive model: **(a)** Parabolic compressive softening; **(b)** Exponential tensile softening (DIANA, 2020)

Timber components, including beams and flooring, were modeled as solid elements with linear elastic properties. Reinforcement bars used in the seismic bands were represented by line elements, adopting a Von Mises plasticity model with isotropic hardening behavior. The hardening relationship between plastic strain and yield stress is illustrated in Figure 5.

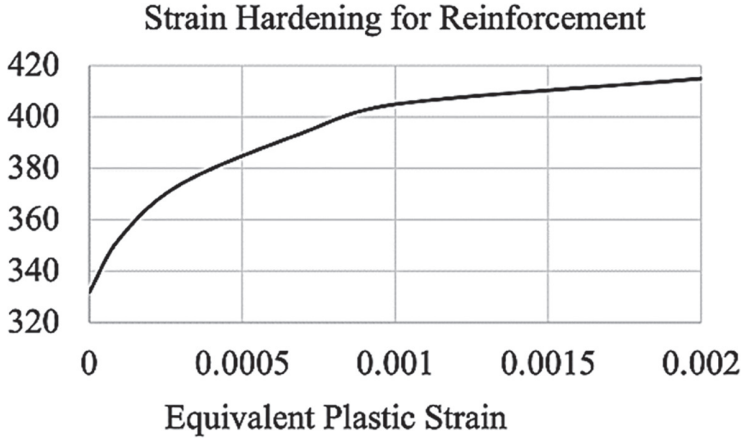

Figure 5: Strain Hardening plot for Fe415 adopted in numerical model (IS 456, 2000)

Concrete bands (sill, lintel, and roof) were also modeled as solid elements using the Total Strain-Based Crack Model, employing the same constitutive definitions for tensile and compressive behavior as used for the masonry walls. The material properties assigned to all components in the models are summarized in Table 1.

Table 1: Material properties adopted in the finite element model.

	Young's Modulus of Elasticity (E)	Mass Density	Poisson's Ratio	Compressive Strength	Compressive Fracture Energy	Tensile Strength	Tensile Fracture Energy
	MPa	Kg/m3	-	MPa	N/m	MPa	N/m
Stone Mud Masonry (Build Change, 2019)	65.1	2200	0.25	2.4	240	0.02	2
Concrete (IS 456, 2000)	22360.7	2500	0.2	20	2000	2.2	220
Timber (IS 883, 2005)	9570	693	0.3	-	-	-	-
Steel (IS 456, 2000)	2,00,000	-	-	-	-	-	-

4. Rayleigh's Damping

The Rayleigh damping model is the most commonly used formulation primarily because of its mathematical convenience and ease of implementation in numerical analysis (Cruz & Miranda, 2017b). Rayleigh damping model accounts for mass proportional damping model and stiffness proportional damping model as illustrated in Figure 6.

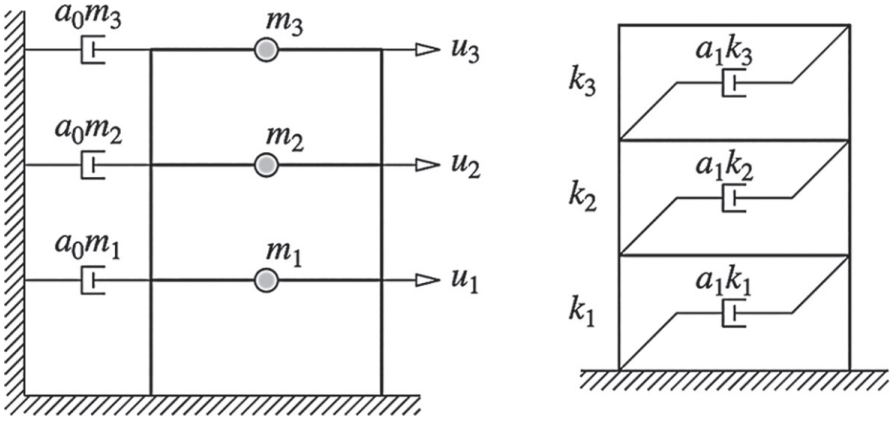

(a) (b)

Figure 6: (a) Mass-proportional damping model and **(b)** Stiffness-proportional damping model (Chopra, 2012)

The Rayleigh damping matrix C is expressed as a linear combination of the mass matrix (M) and the stiffness matrix (K), as illustrated in Figure 7 and the equation below:

$$C = a_0M + a_1K$$

where α_0 and α_1 are the Rayleigh damping coefficients. The following relations at two selected natural circular frequencies ω_i and ω_j were solved to determine α_0 and α_1.

$$2\varsigma = \frac{a_0}{\omega_i} + a_1\omega_i \text{ and } 2\varsigma = \frac{a_0}{\omega_j} + a_1\omega_j$$

Here, ς is the assumed damping ratio.

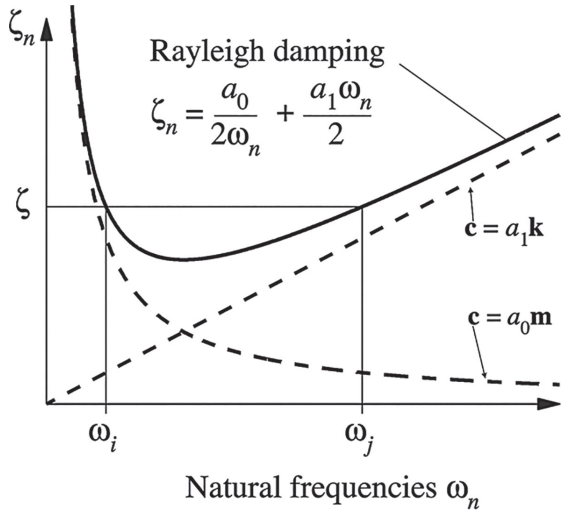

Figure 7: Variation of damping ratio with frequency of the mass-proportional, stiffness-proportional, and Rayleigh damping model (Chopra, 2012)

Solving equations above simultaneously gives:

$$a_0 = \frac{2\varsigma\omega_i\omega_j}{\omega_i+\omega_j} \text{ and } a_1 = \frac{2\varsigma}{\omega_i+\omega_j}$$

In this study, the first natural circular frequency and the frequency corresponding to the mode where the cumulative mass participation factor exceeded 90% were selected for calculating a_0 and a_1(DIANA, 2020; Rahman & Gupta, 2020). These coefficients were computed by DIANA FEA (DIANA, 2020) based on the specified damping ratio and modal information and employed in the respective model.

5. Analysis

5.1. Non-Linear Time History Analysis

To evaluate the seismic response of both unreinforced masonry (URM) and reinforced masonry (RM) structures, nonlinear time history analyses (NLTHA) were performed under ground motion from the 2015 Gorkha Earthquake (Takai et al., 2016), recorded at the KTP station. The analyses were conducted using the Incremental Dynamic Analysis (IDA) procedure (Vamvatsikos & Cornell, 2002), which relates the intensity measure (IM) of a ground motion to the corresponding damage measure (DM) of a structure. In this study, the peak ground acceleration (PGA) was adopted as the IM, and the maximum inter-storey drift ratio (IDR) as the DM.

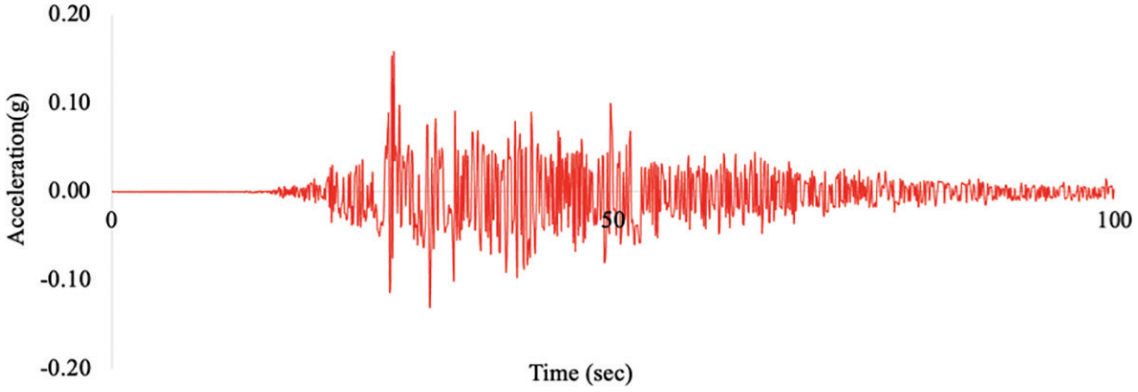

Figure 8: Ground motion acceleration record (Takai et al., 2016)

To capture the full nonlinear response of both models, progressively scaled versions of the selected ground motion were applied. For the URM model, analyses began at a PGA of 0.1 g and increased in increments of 0.1 until the collapse damage limit state defined in Table 2 was reached. For the RM model, scaling started at 0.2 g, following the incremental pattern of 0.2. In total, 149 nonlinear analyses were conducted across the two models and six damping ratios (1% – 6%) to capture their complete dynamic behavior. Both material and geometric nonlinearities, as well as transient dynamic effects, were taken. The Newton–Raphson iterative method ensured convergence, while the Parallel Direct Sparse solver was chosen for the solution of the nonlinear equations.

Table 2: Threshold drift values for damage states (Pema, 2020)

Damage State	Unreinforced Masonry	Reinforced Masonry
Slight Damage (SD)	1/1000 (0.1%)	1/500 (0.2%)
Moderate Damage (MD)	1/750 (0.13%)	1/350 (0.28%)
Extensive Damage (ED)	1/500 (0.2%)	1/150 (0.67%)
Collapse (CL)	1/300 (0.33%)	1/75 (1.33%)

For the URM model, an increase in damping produced a reduction in roof displacement. As shown in Figure 9, the roof displacement under the selected ground motion at 0.40 g decreased from 8.17 mm at 1% damping to 3.91 mm at 6% damping, showing the substantial role of damping in reducing dynamic response.

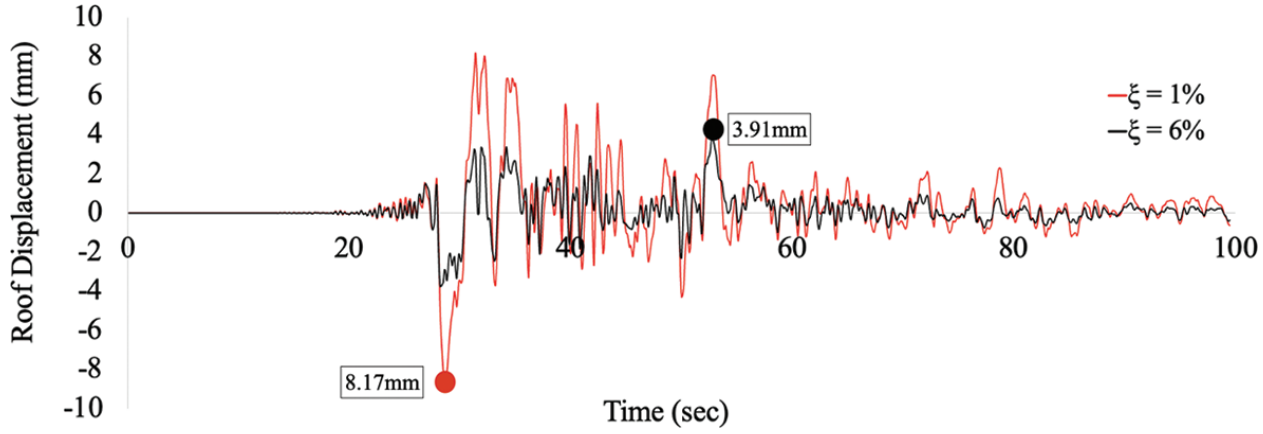

Figure 9: Roof Displacement vs Time plot for URM

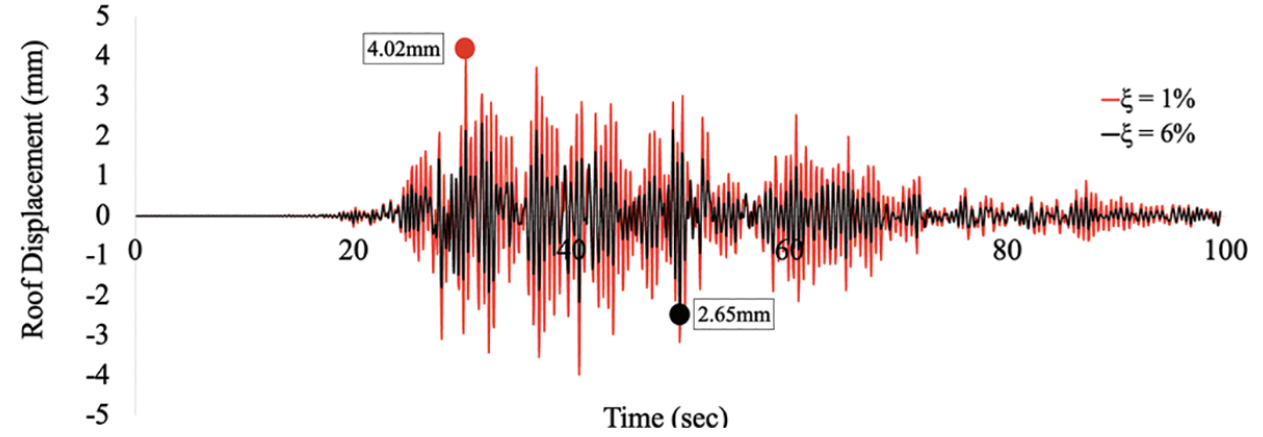

Figure 10: Roof Displacement vs Time plot for RM

For the RM model, a similar decreasing trend was observed, though the variation was less pronounced. Under the same conditions, roof displacement reduced from 4.02 mm at 1% damping to 2.65 mm at 6% damping, as shown in Figure 10. This smaller difference indicates that the inclusion of seismic bands and vertical reinforcement enhanced stiffness and energy dissipation capacity, thereby reducing sensitivity to damping variation.

The structural response was further evaluated in terms of the inter-storey drift ratio (ISD), calculated using:

$$ISD = \frac{\Delta}{h}$$

where h is the corresponding storey height, and Δ represents the relative displacement between consecutive storeys.

The ISD was calculated for two-storey levels, with the larger value adopted as the representative measure of structural damage. This parameter was used as the damage measure (DM) in the fragility analysis. The resulting IDA curves, showing the relationship between PGA and inter-storey drift for both URM and RM structures, are presented in Figure 11. From these curves, it is clear that the response of the URM model diverges noticeably from the initial stage as the intensity increases. In contrast, the RM model exhibits

consistent behavior across all damping levels in the initial range, with variations emerging only at higher intensity levels. These results formed the basis for the fragility curve development.

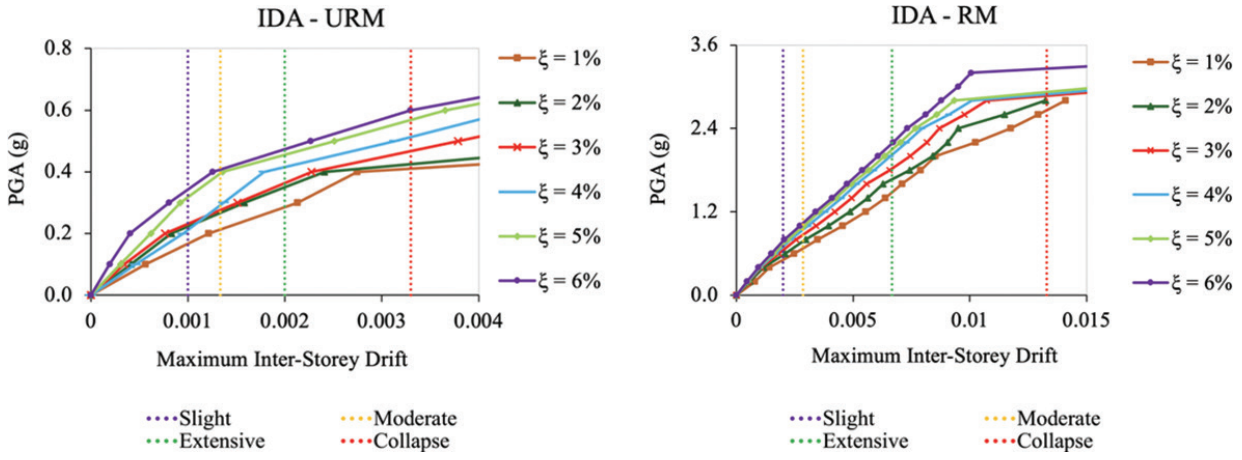

(a) (b)

Figure 11: IDA Curves: (a) URM and (b) RM model

5.2. Fragility Analysis

The fragility curves were developed by plotting the probability of exceeding a defined damage threshold against different levels of ground motion intensity (GMI). These curves provide a representation of the likelihood that a structure will reach or exceed specified damage states under earthquake loading.

To construct fragility curves, the results obtained from the Incremental Dynamic Analysis (IDA) were utilized. Based on the recommendations of Pema (2020), the damage states were defined based on inter-storey drift ratio thresholds as shown in Table 2. The table summarizes the drift limits corresponding to four distinct damage states—slight, moderate, extensive, and collapse—for both unreinforced masonry (URM) and reinforced masonry (RM) structures. These thresholds are limit states in the fragility analysis, enabling the evaluation of the probability of exceedance for each damage level under varying earthquake intensities.

The IDA results were related to the predefined damage states through a fragility function based on the methodology proposed by (Wen et al., 2004) which quantifies the probability of exceeding a given damage threshold at different GM levels. The fragility function is expressed as:

$$P\left(\frac{LS_I}{GM}\right) = 1 - \phi\left(\frac{\lambda_{CL}^{i} - \lambda_{D/GM}}{\beta_{D/GM}}\right)$$

where:

- $P\left(\frac{LS_I}{GM}\right)$ = the probability of exceeding a specific limit state at given ground motion intensity (GM)
- GM = Ground Motion Intensity in g.
- $\phi(\,)$ = the standard normal cumulative distribution function.

- λ_{CL}^{i} = ln (median story drift corresponding to a specific limit state, i).
- $\lambda_{D/GM}$ = ln (calculated median demand story drift for the given GM, obtained from the best-fit power-law line).

$$\lambda_{D/GM} = ln(a_1) + a_2 ln(GM)$$

Further, α_1 and α_2 are constants obtained from linear regression analysis of the logarithmic relationship between storey drift and GM in terms of PGA, and *n* is the number of performance points.

5.2.1. Unreinforced Masonry

The maximum inter-storey drift (ISD) values at different peak ground accelerations (PGA) levels were used to establish a regression relationship between ln(drift) and ln(PGA). This regression enabled the determination of the coefficients $\ln(a_1)$ and a_2. These parameters are essential for developing the fragility curves of both models across the various damping ratios. Table 3 presents the mean, standard deviation, and coefficient of determination (R^2) values for the URM model at all six damping levels, while Figure 12 illustrates the regression plot corresponding to the 3% damping ratio. All R^2 values exceed 0.90, showing a strong correlation and a reliable regression fit (Schober et al., 2018).

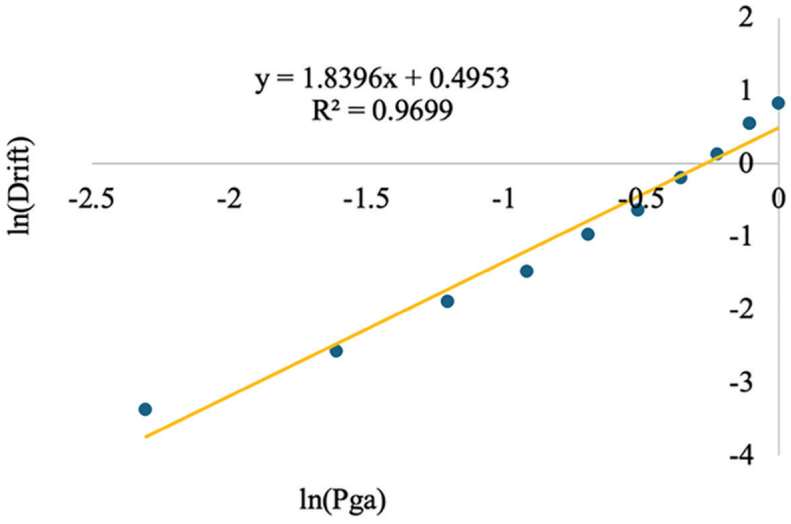

Figure 12: Regression curve of ln(drift) vs ln(PGA) for damping varied URM model

Table 3: Mean, standard deviation, and goodness of fit parameters for damping varied URM model

Damping	$ln(a_1)$	a_2	β	R^2
1%	0.3756	1.4782	0.4924	91.67%
2%	0.9751	2.0387	0.8253	95.83%
3%	**0.4953**	**1.8396**	0.6798	**96.99%**
4%	0.0957	1.5349	0.5544	94.75%
5%	-0.0671	1.6624	0.8384	95.65%
6%	-0.1073	1.8259	1.0664	97.73%

**Figure 12 shows the plot of parameters highlighted in bold.*

As observed from the fragility curves, the response of the URM model varies with damping ratio. At slight and moderate damage states, the curves for 2%, 3%, and 4% damping show similar behavior, indicating minimal sensitivity in this range. For the extensive damage state, only the 3% and 4% curves remain close together, while the 2% curve begins to diverge with higher probability. At the collapse damage state, the 3% and 4% curves separate slightly, and the 2% curve is closer to the 1% curve, reflecting higher vulnerability at lower damping. The largest differences in response are seen at the extreme damping values of 1% (lower) and 6% (higher), highlighting the pronounced effect of very low and very high damping on structural fragility.

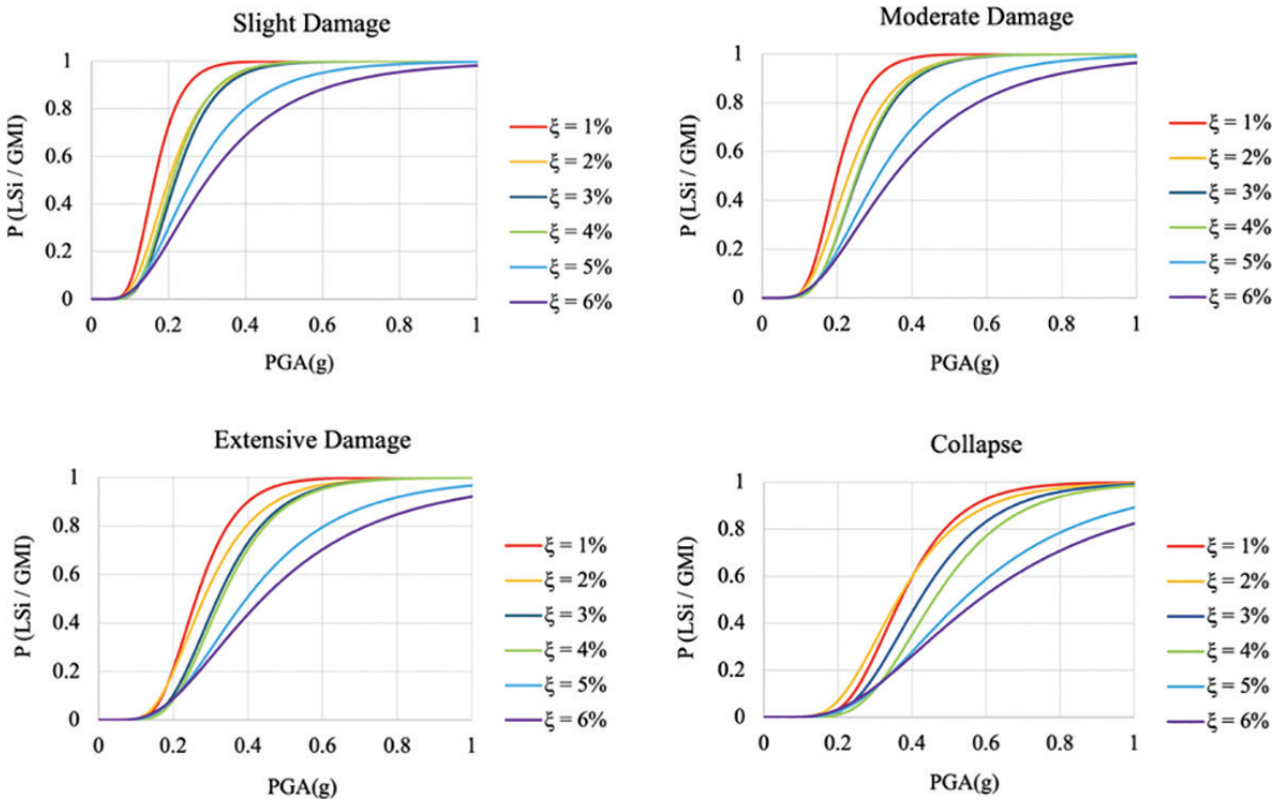

Figure 13: Fragility Curves for URM model at different damping levels

5.2.2. Reinforced Masonry

Similarly, for the RM model, the regression coefficients $\ln(a_1)$ and a_2 were obtained from the maximum inter-storey drift values at different PGA levels. Table 4 summarizes the mean, standard deviation, and coefficient of determination (R^2) for all six damping levels, while Figure 14 presents the regression plot for the 3% damping ratio.

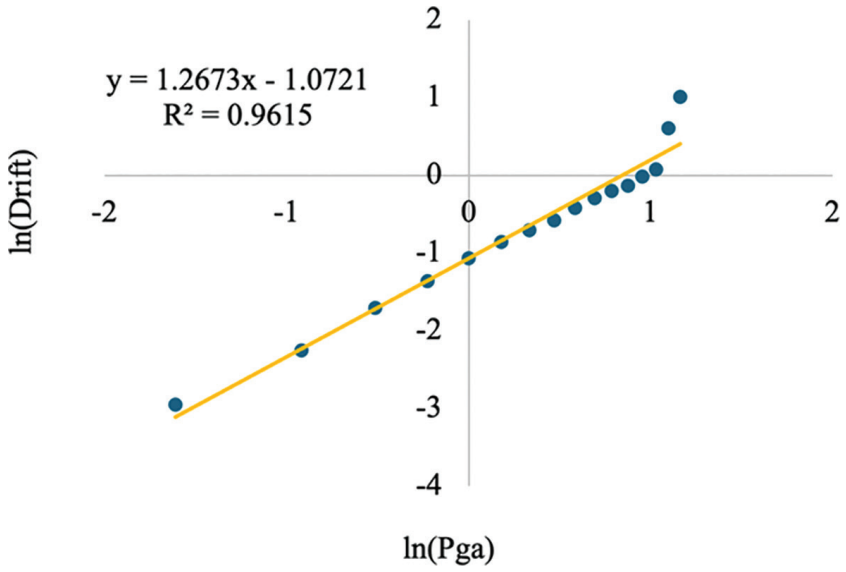

Figure 14: Regression curve of ln(drift) vs ln(PGA) for damping varied RM model

Table 4: Mean, standard deviation, and goodness of fit parameters for damping varied RM model

Damping	$ln(a_1)$	a_2	β	R^2
1%	-0.8315	1.0993	0.8813	99.6%
2%	-0.9846	1.1701	1.0376	99.71%
3%	**-1.0721**	**1.2673**	1.0805	**96.15%**
4%	-1.1541	1.247	1.1701	96.23%
5%	-1.2042	1.2372	1.2247	96.45%
6%	-1.2558	1.2578	1.2376	94.09%

**Figure 14 shows the plot of parameters highlighted in bold.*

For the RM model, the fragility curves at different damage states for different damping ratios are compared in Figure 15. Here, the variation in response decreases progressively toward the collapse damage state. At slight, moderate, and extensive damage levels, the 1% damping curve remains the most separated, while 2% and 3% are close together and 5% and 6% form another cluster, with 4% positioned near the higher damping group. Overall, the variation across damping levels is less pronounced than in the URM model. At the collapse damage state, all damping level curves essentially overlap, showing that the reinforced structure's

response is relatively insensitive to damping variation at extreme damage levels.

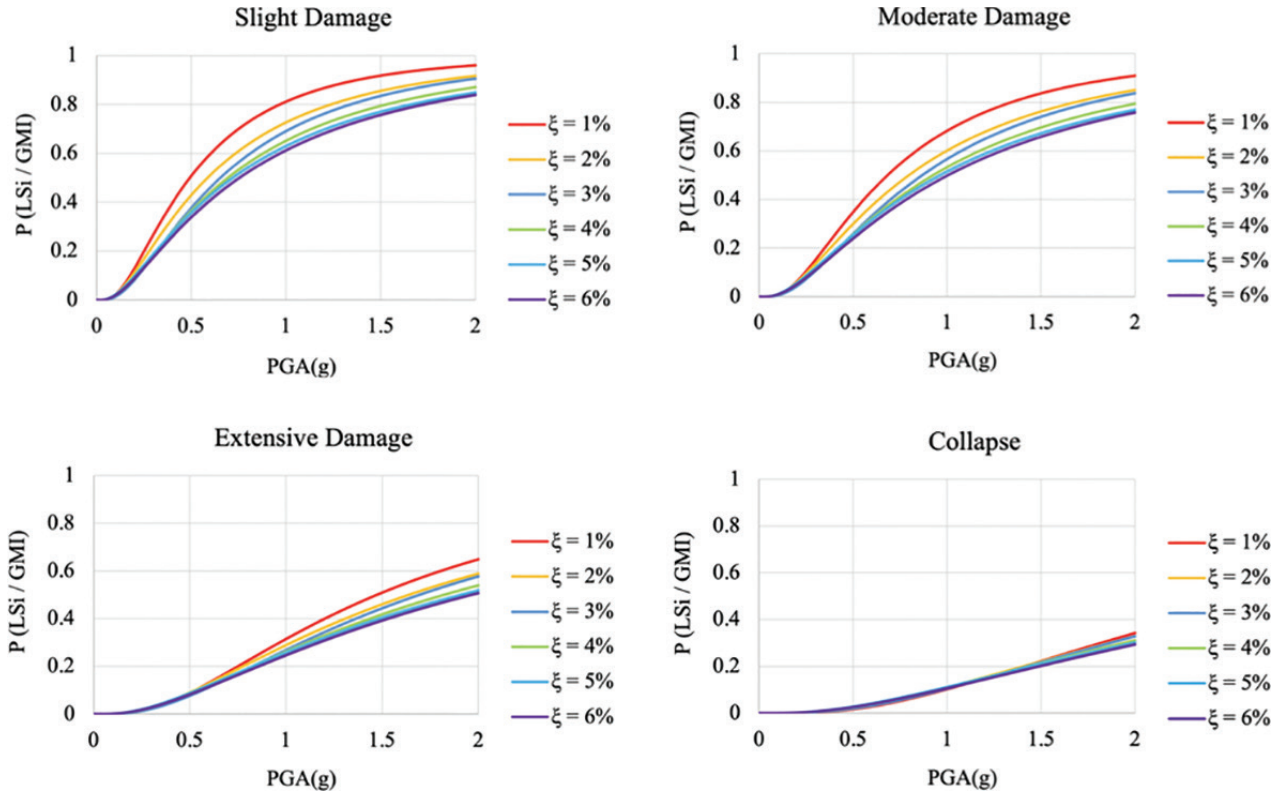

Figure 15: Fragility Curves for RM at different damping levels

The results from the fragility analyses showed that the lateral response of unreinforced masonry (URM) structures is highly sensitive to the damping ratio, particularly at lower and higher extremes (1% and 6%). This suggests that accurate estimation of damping is critical for such structures. Therefore, for historic or culturally significant URM buildings, which may lack reinforcement and may be vulnerable to seismic damage, material testing or ambient vibration tests are recommended to determine the actual damping characteristics for reliable seismic assessment.

In contrast, for reinforced masonry (RM) structures, the variation in structural response across different damping ratios decreases progressively toward the collapse damage state. At the collapse level, damping has a relatively minor effect, and the fragility curves for all damping ratios largely overlap. This shows that, for reinforced residential buildings, assuming a standard damping ratio within the range of 2–5%, as suggested by (Anderson & Brzev, 2009), is sufficient for practical design purposes, even when assessing extreme damage or collapse levels.

Overall, the findings focused on the need for site- and material-specific damping evaluation for unreinforced masonry, especially in historic structures, whereas for reinforced masonry, simplified assumptions for damping are generally enough at high damage levels.

The present study employs simplified macro-models of URM buildings and does not account for soil–structure interaction, localized material nonlinearity, or detailed micro modeling of masonry units and mortar. Future work could follow micro modeling techniques along with soil–structure interaction effects to

better capture local failure mechanisms and enhance the accuracy of fragility predictions.

6. Comparative Study of URM and RM

While the primary objective of this study is to examine the variation of structural fragility with respect to different damping ratios, a comparative assessment between Unreinforced Masonry (URM) and Reinforced Masonry (RM) models is also studied in this section. Previous studies have addressed this topic. For example, the DUDBC (DUDBC, 2015b) Masonry Guidelines provide a clear difference between the seismic behavior of unreinforced and reinforced masonry. (Ban et al., 2024) evaluated the effectiveness of various seismic strengthening elements, highlighting the improvement in global stiffness and ductility due to reinforcement. Similarly, (Upadhyay et al., 2025) compared the seismic performance of unreinforced masonry with its retrofitted and reinforced models, demonstrating enhanced resilience under seismic loading.

In this paper, the comparison between URM and RM is conducted based on fragility curves developed at a 5% damping ratio, as shown in Figure 16.

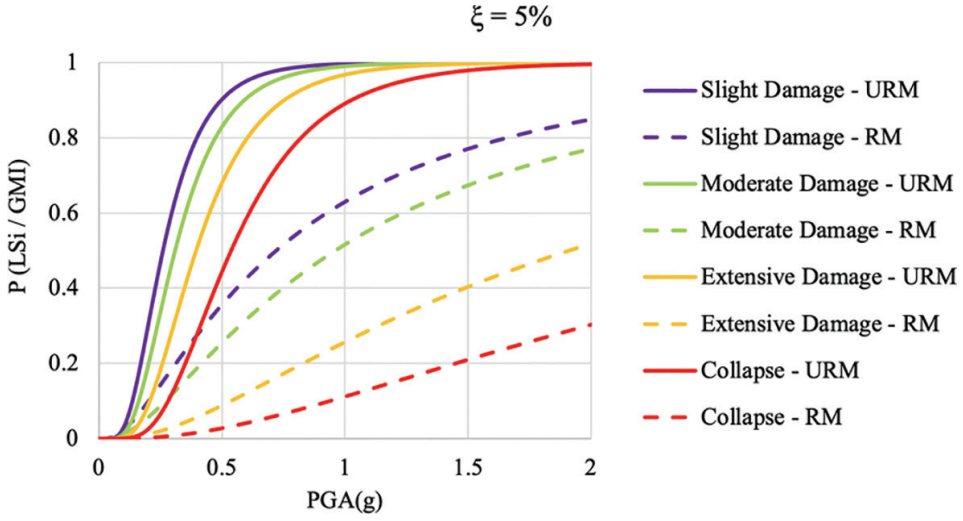

Figure 16: Fragility curves for URM and RM at 5% damping level

The results in Table 5 show the probability of damage exceedance for both URM and RM models at a peak ground acceleration (PGA) of 0.40 g and 5% damping. The PGA value of 0.40 g is selected because it represents the maximum design-level ground acceleration mentioned in NBC 105:2020 (NBC, 2020) for high seismic hazard zones of Nepal. It is clear that reinforcement significantly reduces the likelihood of damage across all limit states. For slight damage, the probability decreases from 0.802 in URM to 0.276 in RM, showing a clear improvement in initial stiffness and energy dissipation capacity.

Table 5: Probability of exceedance of drift state at intensity of 0.40g PGA

Damage State	Probability of exceedance of drift limit state	
	URM (ξ=5%)	RM (ξ=5%)
Slight Damage	0.802	0.276
Moderate Damage	0.693	0.187
Extensive Damage	0.509	0.057
Collapse	0.278	0.016

As the severity of damage increases, this difference becomes even more clear. The probability of moderate damage reduces from 0.693 to 0.187, and extensive damage from 0.509 to 0.057, demonstrating that reinforcement effectively delays the onset of structural degradation. The collapse probability shows the greatest reduction—from 0.278 for URM to 0.016 for RM—highlighting the significant enhancement in overall seismic safety and structural integrity. Overall, the results confirm that reinforcement provides consistent and progressive protection against increasing seismic intensity, reducing both vulnerability and collapse risk.

7. Conclusion

This paper studied the influence of Rayleigh damping variation on the seismic fragility of unreinforced masonry (URM) and reinforced masonry (RM) buildings through numerical macro-model analysis. For this, damping ratios were varied from 1% to 6%, and incremental dynamic analyses (IDA) were performed to develop corresponding fragility curves. The objective was to study how variations in Rayleigh damping parameters affect the predicted damage probability and seismic performance of masonry structures. The result found following major points: -

- With increase in damping ratios, the roof displacement was reduced along with overall seismic response. The URM model was sensitive to Rayleigh damping variation, showing that very low or very high damping assumptions can highly alter the predicted fragility and damage probabilities of URM buildings.
- In contrast, for the RM model, the influence of damping variation decreased progressively toward the collapse damage state. This suggests reduced dependence on damping assumptions at higher deformation levels. Structural stiffness and reinforcement resulted in smaller variations in fragility curves due to energy dissipating capacity.
- Reinforced masonry consistently performed better than unreinforced masonry across all damage states, highlighting its superior seismic performance.

Overall, the findings suggest that Rayleigh damping parameters have a notable effect on the fragility estimation of unreinforced masonry, suggesting the need for site-specific damping characterization, especially for historic structures. For reinforced masonry, standard guideline-based damping ratios are generally sufficient. This can still be true for assessing collapse-level fragility. The outcomes of this study highlight the importance of damping sensitivity evaluation in seismic fragility assessment and contribute to improving the reliability of numerical modeling for masonry structures.

References

Acharya, P., Sharma, K., & Liu, F. (2024). Türkiye's Road to Recovery after the 2023 Kahramanmaras Earthquake: Lessons from Chile, Japan, and Nepal. *Natural Hazards Review, 25*(4), 04024031. https://doi.org/10.1061/NHREFO.NHENG-1985

Adhikari, R. K., & D'Ayala, D. (2020). 2015 Nepal earthquake: seismic performance and post-earthquake reconstruction of stone in mud mortar masonry buildings. *Bulletin of Earthquake Engineering, 18*(8), 3863-3896. https://doi.org/10.1007/s10518-020-00834-y

Alipour, A., & Zareian, F. (2008, 2008). Study rayleigh damping in structures; uncertainties and treatments.

Anderson, D., & Brzev, S. (2009). *Seismic design guide for masonry buildings* (Vol. 22). Canadian Concrete Masonry Producers Association Toronto, ON.

Ban, S., Shrestha, K. C., & Bastola, S. (2024). Seismic performance assessment of stone masonry buildings: Efficacy of various strengthening elements. *Journal of Building Engineering, 96*, 110380. https://doi.org/10.1016/j.jobe.2024.110380

Build Change. (2019). Laboratory Test Report on Stone Masonry in Mud Mortar, 2019. In.

Chopra, A. K. (2012). *Dynamics of Structures*. Pearson Education. https://books.google.com.np/books?id=eRcvAAAAQBAJ

Cruz, C., & Miranda, E. (2017a). Evaluation of damping ratios for the seismic analysis of tall buildings. *Journal of structural engineering, 143*(1), 04016144.

Cruz, C., & Miranda, E. (2017b). Evaluation of the Rayleigh damping model for buildings. *Engineering Structures, 138*, 324-336.

D'Alessandro, A., & Fusi, S. (2025). Seismic Risk Prevention Policies in Italy, Japan, the United States (California), Chile, Turkey, and Greece: A Comparative Analysis of Prevention Strategies. *Japan, the United States (California), Chile, Turkey, and Greece: A Comparative Analysis of Prevention Strategies*.

DIANA. (2020). *DIANA User's Manual. Release 10.5, TNO, Netherlands*.

DUDBC. (2015a). Design Catalogue for Reconstruction of Earthquake Resistant Houses Volume I, Department of Urban Development and Building Construction, Ministry

Of Urban Development, Government of Nepal, Kathmandu, 2015. In.

DUDBC. (2015b). Seismic Retrofitting Guidelines of Buildings in Nepal - Masonry, 2015. https://www.dudbc.gov.np/content/2386/2386-seismic-retrofitting-guideline/

Galvez, F., Sorrentino, L., Dizhur, D., & Ingham, J. M. (2022). Damping considerations for rocking block dynamics using the discrete element method. *Earthquake Engineering & Structural Dynamics, 51*(4), 935-957.

Gautam, D. (2018). Observational fragility functions for residential stone masonry buildings in Nepal. *Bulletin of Earthquake Engineering, 16*(10), 4661-4673.

Giordano, N., De Luca, F., & Sextos, A. (2021). Analytical fragility curves for masonry school building portfolios in Nepal. *Bulletin of Earthquake Engineering, 19*(2), 1121-1150. https://doi.org/10.1007/s10518-020-00989-8

Guragain, R., Dixit, A. M., & Meguro, K. (2012, 2012). Development of fragility functions for low-strength masonry buildings in Nepal using applied element methods.

Hall, J. F. (2006). Problems encountered from the use (or misuse) of Rayleigh damping. *Earthquake Engineering & Structural Dynamics, 35*(5), 525-545.

IS 456. (2000). *Indian Standard Plain and Reinforced Concrete - Code of Practice, Bureau of Indian Standards, New Delhi, India, 2000, 2000;(July)*.

IS 883. (2005). *Design of Structural Timber in Building -Code of Practice, Bureau of Indian Standards, New Delhi, India, 2005*.

Jaishi, B., Ren, W.-X., Zong, Z.-H., & Maskey, P. N. (2003). Dynamic and seismic performance of old multi-tiered temples in Nepal. *Engineering Structures, 25*(14), 1827-1839. https://doi.org/10.1016/j.engstruct.2003.08.006

Khadka, B. (2020). Mud masonry houses in Nepal: A detailed study based on the entire reconstruction scenario in 31 earthquake-affected districts. Structures,

NBC. (2015). *NBC 202, Guidelines on: Load Bearing Masonry, Department of Urban Development and Building Construction, Government of Nepal, Kathmandu, 2015*. https://www.moud.gov.np/storage/listies/July2019/NBC_202_2015_Guidline_on_Load_Bearing_Masonry.pdf

NBC. (2020). *NBC 105:2020, Seismic Design of Buildings in Nepal, Department of Urban Development and Building Construction, Government of Nepal*.

Ortega, J., Vasconcelos, G., Rodrigues, H., & Correia, M. (2019). A vulnerability index formulation for the seismic vulnerability assessment of vernacular architecture. *Engineering Structures, 197*, 109381.

Pema. (2020). *Seismic Evaluation and Retrofitting of Traditional Bhutanese Stone Masonry Residential House, Synopsis of IISEE-GRIPS Master Report, 2020. Published online.*

Rahman, M. H., & Gupta, C. (2020). Computation of Rayleigh damping coefficient of a rectangular submerged floating tunnel (SFT). *SN Applied Sciences*, *2*(5), 936.

Ram, T. D., & Wang, G. (2013). Probabilistic seismic hazard analysis in Nepal. *Earthquake Engineering and Engineering Vibration*, *12*(4), 577-586. https://doi.org/https://doi.org/10.1007/s11803-013-0191-z

Schober, P., Boer, C., & Schwarte, L. A. (2018). Correlation Coefficients: Appropriate Use and Interpretation. *Anesthesia & Analgesia*, *126*(5). https://doi.org/10.1213/ANE.0000000000002864

Spears, R. E., & Jensen, S. R. (2012). Approach for selection of Rayleigh damping parameters used for time history analysis. *Journal of Pressure Vessel Technology*, *134*(6), 061801.

Takai, N., Shigefuji, M., Rajaure, S., Bijukchhen, S., Ichiyanagi, M., Dhital, M. R., & Sasatani, T. (2016). Strong ground motion in the Kathmandu Valley during the 2015 Gorkha, Nepal, earthquake. *Earth, Planets and Space*, *68*(1), 10. https://doi.org/10.1186/s40623-016-0383-7

Upadhyay, M., Kafle, P., Ban, S., & Khakurel, S. (2025). Seismic enhancement of community housing in Nepal's mid-Himalayas: Retrofitting and reconstruction scenarios. https://doi.org/10.5459/bnzsee.1733

Vamvatsikos, D., & Cornell, C. A. (2002). Incremental dynamic analysis. *Earthquake Engineering & Structural Dynamics*, *31*(3), 491-514. https://doi.org/10.1002/eqe.141

Wang, M., Liu, K., Lu, H., Shrestha, H., Guragain, R., Pan, W., & Yang, X. (2018). In-plane cyclic tests of seismic retrofits of rubble-stone masonry walls. *Bulletin of Earthquake Engineering*, *16*(5), 1941-1959. https://doi.org/10.1007/s10518-017-0262-z

Wen, Y. K., Ellingwood, B. R., & Bracci, J. (2004). *Y.K. Wen, B.R. Ellingwood, J. Bracci, Vulnerability Function Framework for Consequence-Based Engineering, Mid-America Earthq Cent Proj, 2004, pp. 1–101.*